RESPONSE OF LOW VOLTAGE GRIDS WITH CONNECTED PROSUMERS TO A VOLTAGE DIP

Daniel-Leon SCHULTIS
TU Wien – Austria
daniel-leon.schultis@tuwien.ac.at

Albana ILO
TU Wien – Austria
albana.ilo@tuwien.ac.at

ABSTRACT

The increasing penetration of rooftop PV-systems modifies the reactive power flow through the distribution transformer. Additionally, the dynamic behaviour of the low voltage grid is mainly defined by the dynamics of the PV-systems and load devices. This paper studies the reactive power response of low voltage grids with connected prosumers to a voltage dip provoked by a three-phase fault in the superordinate grid. A detailed prosumer and PV-system model is used to analyse the reactive power contribution of a low voltage grid in stabilizing the situation during and after the fault. Three scenarios are considered: without PV-systems; with PV-systems; and with PV-systems upgraded with dynamic voltage support. Results show that, compared to the case without PV-systems, the integration of PV-systems increases the Q-flow from the medium into the low voltage grid and the voltages in low voltage grid. If PV-systems are upgraded with dynamic voltage support, the low voltage grid behaviour changes during the voltage dip: it produces reactive power thus supporting the voltage recovery process of the superordinate grid, but simultaneously, it has lower voltages. Furthermore, the post-fault stabilization process in low voltage grid is significantly delayed in this case.

INTRODUCTION

Voltage dips appear and propagate on the grid after a short circuit in transmission level, big motor starting or transformer energizing. The large scale presence of the distributed generators (DG) mitigates the voltage dip, because they inject power into the grid. To increase the voltage stability, low-voltage-fault-ride-through (LVFRT) and dynamic-voltage-support (DVS) of DGs are suggested by several grid codes [1, 2]. LVFRT requires the generation unit to stay grid-connected for a minimum time-interval also during severe voltage dips. DVS requires it to inject reactive power during LVFRT.

Many works have used a simplified lumped model of the load devices, DGs and the low voltage grid to study the stability of power systems [3]. An investigation of the detailed low voltage grid behaviour with large rooftop PV share and different load devices during a voltage dip is not performed in the past.

This paper analyses for the first time the reactive power response of low voltage grids (LVG) with connected prosumers (with rooftop PV-systems) to a voltage dip provoked by a three-phase fault in superordinate grids. Firstly, the simulation models of the load devices, PV-systems and the low voltage grid are described. Secondly, the simulation scenarios are defined. Then, the simulation results are analysed and finally, conclusions are drawn.

METHODOLOGY

The analyses in this paper is focused on voltage dips caused by a three-phase fault in transmission level, Figure 1. The load devices, PV-systems and low voltage grid are modelled in detail. This is important because low voltage grids have a special structure. The customer plants and thus also the DGs (rooftop PVs) are connected almost homogeneously in relative small distances to each other at the low voltage feeders. They operate under different voltage conditions and thus the connected devices behave differently. For simplicity, only the low voltage grid is modelled and the voltage dip is applied at the primary side of the distribution transformer (DTR). The load devices and PV installations are supposed to be equally distributed among three phases, thus the analyses is restricted to the positive sequence.

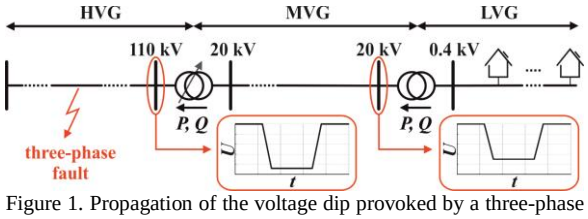

Figure 1. Propagation of the voltage dip provoked by a three-phase fault in transmission level.

MODEL DESCRIPTION

Prosumer and low voltage grid models are described in the following. Both models are three phase models. As simulation platform is used the "Simscape Power Systems" toolbox in Matlab/Simulink R2018b.

The load concept is quite broad. Sometimes, the load represents the power consumption of a motor or of an entire grid part with all thereto connected elements. In the last case, the term lumped load is more accurate, because the static and dynamic behaviour of the load is defined by the behaviour of all connected elements. Therefore, the large-scale integration of rooftop PV-systems modifies the lumped load seen from the transmission grid.

Prosumer model

Prosumers have load devices and electricity production facilities. In this study we are restricted to rooftop PV-systems. The dynamic behaviour of the load is crucial for

the voltage stability of power systems [4]. Due to the low R/X-ratio in high voltage grids, the reactive power part of the load has the highest impact on it. Regarding the residential load class, loads can be classified into resistive, switched-mode-power-supply (SMPS) and single-phase induction motor (SPIM) loads, as well as efficient lighting devices [5]. Critical loads with respect to dynamic voltage stability are SPIM-driven residential air-conditioners with low inertia and constant torque, which lack an under-voltage protection. These motors can stall within a few cycles in response to voltage dips due to a fault in transmission level. They require typically 5 to 6 times their steady-state current in this locked-rotor condition until they get disconnected from the grid by their thermal protection, which can take from 3 to 20 seconds. This further aggravates the initial voltage depression in transmission level and leads to the well-known phenomenon of fault-induced-delayed-voltage-recovery [6]. The other SPIM-driven home devices, which show a higher inertia, do not stall during the short existing time of the voltage dip. Therefore, they are not considered in this study.

Figure 2a) shows the structure of the prosumer model. It consists of one three-phase PV-inverter and three different load types: one three-phase resistive-, one three-phase

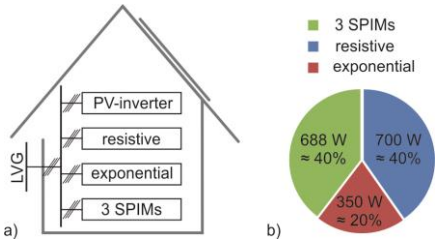

Figure 2. Prosumer model overview: a) model structure; b) composition of the total prosumer load under nominal conditions.

exponential- and three SPIM-loads. Figure 2b) presents the total load composition. The resistive and motor load are the dominant part of the load, each with about 40%. Meanwhile, about 20% of the total load has an exponential character. Efficient lighting devices are neglected, since the selected scenarios are significant during the day, when no electrical lightning is necessary.

Load modelling

Three load types are modelled: resistive, exponential, and SPIM.

- Three-phase resistive load model represents resistive heating and cooking. It consists of three-phase grounded resistors with $\boldsymbol{R_{wye} = 228.57\ \Omega}$.

- Three-phase exponential load model represents SMPS loads like televisions, desktop computers, monitors, printers, etc. This load model consumes active and reactive power according to equations (1) and (2). It only absorbs positive sequence currents, even under unbalanced voltage conditions.

$$P_{SMPS} = \mathrm{P_{0,SMPS}} \cdot \left(\frac{U}{\mathrm{U_n}}\right)^{\mathrm{n_p}} \quad (1)$$

$$Q_{SMPS} = \mathrm{Q_{0,SMPS}} \cdot \left(\frac{U}{\mathrm{U_n}}\right)^{\mathrm{n_q}} \quad (2)$$

where:

$\mathrm{P_{0,SMPS}}$	…	active power consumption at nominal voltage
$\mathrm{Q_{0,SMPS}}$	…	reactive power consumption at nominal voltage
$\mathrm{n_p}$	…	active power exponent
$\mathrm{n_q}$	…	reactive power exponent
U	…	magnitude of positive-sequence voltage

The SMPS devices are assumed to have passive power factor correction, thus $\mathrm{n_p} = 0$ and $\mathrm{n_q} = -0.5$; power factor at nominal voltage is set to $\cos\varphi_{0,\mathrm{SMPS}} = 0.97$ capacitive [5], thus $\mathrm{Q_{0,SMPS}} = \mathrm{P_{0,SMPS}} \cdot \tan(\varphi_{0,\mathrm{SMPS}})$. Active power consumption at nominal voltage is set to $\mathrm{P_{0,SMPS}} = 350$ W.

- Single-phase induction motor model represents motor-driven mechanical loads with very low inertia, as compressors of air-conditioners and refrigerators, for instance. These loads are typically supplied by single-phase squirrel-cage induction motors with start- and run-capacitors [7]. The generic model of a squirrel-cage SPIM is shown, including normalized voltage, flux linkage, torque and motion equations, as follows [8]:

Voltage equations:

$$u_{qs} = \mathrm{r_s} i_{qs} + \frac{d\psi_{qs}}{dt}$$
$$u_{ds} = \mathrm{r_S} i_{ds} + \frac{d\psi_{ds}}{dt}$$
$$0 = \mathrm{r'_r} i'_{qr} + \frac{d\psi'_{qr}}{dt} - \frac{1}{\mathrm{n}}\omega_r \psi'_{dr}$$
$$0 = \mathrm{r'_R} i'_{dr} + \frac{d\psi'_{dr}}{dt} + \mathrm{n}\omega_r \psi'_{qr}$$

where:

u_{qs}, u_{ds}	…	q- and d-axis stator voltage
i_{qs}, i_{ds}	…	q- and d-axis stator current
i'_{qr}, i'_{dr}	…	q- and d-axis rotor current
ψ_{qs}, ψ_{ds}	…	q- and d-axis stator flux
ψ'_{qr}, ψ'_{dr}	…	q- and d-axis rotor flux
$\mathrm{r_s}, \mathrm{r_S}$	…	main and auxiliary winding stator resistance
$\mathrm{r'_r}, \mathrm{r'_R}$	…	main and auxiliary winding rotor resistance
n	…	turn ratio (auxiliary turns per main turn)
ω_r	…	electrical angular velocity of rotor
t	…	time

Flux linkage equations:

$$\psi_{qs} = (\mathrm{l_{ls}} + \mathrm{l_{ms}}) i_{qs} + \mathrm{l_{ms}} i'_{qr}$$
$$\psi_{ds} = (\mathrm{l_{lS}} + \mathrm{l_{mS}}) i_{ds} + \mathrm{l_{mS}} i'_{dr}$$
$$\psi'_{qr} = (\mathrm{l'_{lr}} + \mathrm{l_{ms}}) i'_{qr} + \mathrm{l_{ms}} i_{qs}$$
$$\psi'_{dr} = (\mathrm{l'_{lR}} + \mathrm{l_{mS}}) i'_{dr} + \mathrm{l_{mS}} i_{ds}$$

where:

$\mathrm{l_{ls}}, \mathrm{l_{lS}}$	…	main and auxiliary winding stator leakage inductance
$\mathrm{l'_{lr}}, \mathrm{l'_{lR}}$	…	main and auxiliary winding rotor leakage inductance
$\mathrm{l_{ms}}, \mathrm{l_{mS}}$	…	main and auxiliary winding magnetizing inductance

Torque and motion equations:

$$T_e = \mathrm{p} \cdot \left(\mathrm{n}\psi'_{qr} i'_{dr} - \frac{1}{\mathrm{n}}\psi'_{dr} i'_{qr}\right)$$
$$\frac{d\omega_m}{dt} = \frac{T_e - T_m}{2\mathrm{H}}$$
$$\omega_r = \mathrm{p} \cdot \omega_m$$

where:

p	…	number of pole pairs
T_e	…	electrical torque
T_m	…	mechanical torque
H	…	inertia of rotor and mechanical load
ω_m	…	mechanical angular velocity of rotor

Table 1 in the Appendix shows the parameters which are used for the SPIM model. If rotor speed drops below zero, the SPIM model enters the locked-rotor-mode, where rotor speed is kept at zero for the remaining simulation time. Thermal protection is not considered since only a short time period after the fault is analysed.

Three-phase photovoltaic inverter model

Figure 3 shows the structure of the simplified three-phase PV-inverter model. The complete DC-side of the PV-

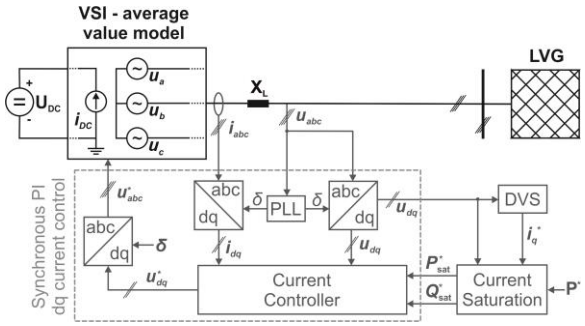

Figure 3. Structure of the simplified three-phase PV-inverter model

system is modelled as an ideal DC voltage source with $U_{DC} = 500$ V. The assumption of constant DC voltage is justified by the large DC-link capacitor and the DC voltage controller of real PV-systems [9]. The voltage source inverter (VSI) is modelled with its average value model. The filter reactance is set to $X_L = 1\,\Omega$. The synchronous PI dq-current control for three-phase voltage-source grid converters is used [10]. It is assumed that LVFRT ensures that the PV-inverters stay grid-connected for the considered time horizon. The inverter rating is set to $S_r =$ 4 kVA, and the active power set-point to $P^* = 4$ kW. The model can be simulated in two modes:

- without DVS → i_q^* is set to zero for the complete time horizon.

- with DVS → the reactive current set-point (i_q^*) is initially set to zero; if the magnitude of the local voltage $|u_{dq}|$ drops below 0.6 pu, i_q^* is set to rated current, and if voltage returns to a value larger than 0.8 pu, it is set to zero again.

The active power set-point is dynamically modified by the "Current Saturation"-block to prevent an exceedance of the inverter's rated current (I_r).

Grid model

Figure 4 shows the simplified one-line diagram of the LVG model. It is a theoretical grid with two feeders with an identical topology; one realized with cables and the other with overhead lines. Each feeder has a length of 1.63 km and supplies 20 rural residential customers. Line segments are modelled as PI-elements with the parameters shown in Tables 2 and 3 in the Appendix. The LVG is connected to the slack node, which is an ideal 50 Hz

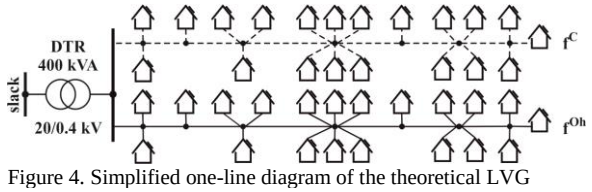

Figure 4. Simplified one-line diagram of the theoretical LVG

positive sequence voltage source, through a 20 kV/0.4 kV, 400 kVA DTR.

SCENARIO DEFINITION

The behaviour of LVG during and after a three-phase fault in transmission level is studied by applying the voltage dip shown in Figure 5 at the slack node of the LVG model.

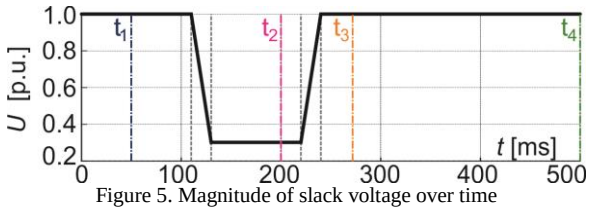

Figure 5. Magnitude of slack voltage over time

This voltage dip is applied for three different scenarios:

Scenario 1: No PV-systems
Scenario 2: PV-systems
Scenario 3: DVS upgraded PV-systems

SIMULATION RESULTS

In all considered scenarios, the applied voltage dip causes all SPIMs to stall. The active (P) and reactive (Q) power behaviour of the whole LVG and separate devices like SPIMs, PVs, conductors etc. is presented in Figures 6 and 7. Therein, consumption of power is counted as positive and production as negative. The SPIMs show a capacitive behaviour at the beginning of the voltage dip, Figure 7, that is reflected also in the LVG behaviour, Figure 6. The post-fault stabilization of the LVG is characterised by an active and reactive power oscillation that begins at t = 220ms.

Figure 6 shows the P- and Q-flows at the DTR primary side for all considered scenarios. Figure 6a) shows the scenario without PV-systems. The load is supplied through the grid. The load power consumption decreases during the voltage dip and drastically increases after voltage recovery. P and Q reach 212% and 1355% of the pre-fault values, respectively. The LVG behaviour quickly stabilizes after voltage recovery ($t \geq$ 240ms). If PV-systems are installed, P flows from the LVG into the medium voltage grid (MVG) before and during the voltage dip, Figure 6b). After voltage recovery, the P-flow reverses. The pre- and post-fault Q-flow is higher compared to the previously discussed case. The post-fault stabilization of the LVG reactive power consumption is slightly delayed by the PV-systems. If PV-systems are

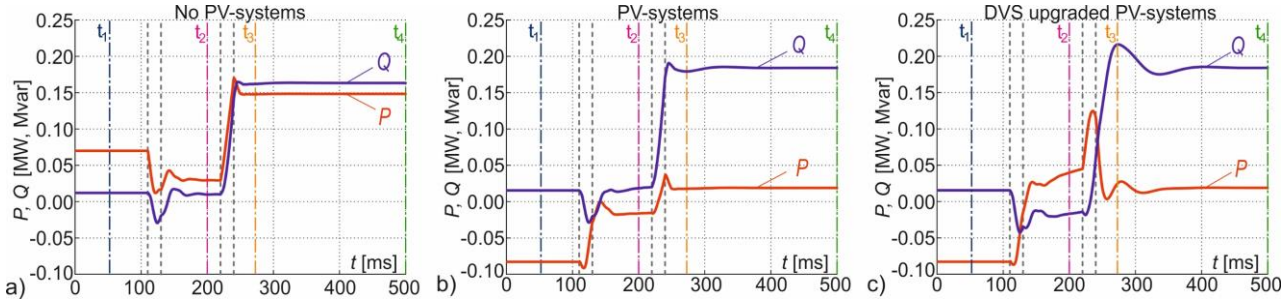

Figure 6. *P*- and *Q*- flows at DTR primary side for different scenarios: a) no PV-systems; b) PV-systems; c) DVS upgraded PV-systems.

DVS upgraded, the LVG behaviour changes during and directly after the fault, Figure 6c). During the voltage dip, the LVG consumes *P* from the MVG but injects *Q* into it. For $t \leq 110$ms and $t \geq 500$ms, the LVG behaviour is similar to the case where PV-systems are not DVS upgraded. The post-fault stabilization of both, LVG active and reactive power consumption, is significantly delayed by the DVS upgraded PV-systems. The *P*- and *Q*-consumption reach their maximum values of about 660% and 117% of the stabilized post-fault values, at t =236ms and t =274ms, respectively. Figure 7 shows *Q*-consumption or -injection of different devices for different scenarios. Figure 7a) present the scenario without PV-systems. The pre- and post-fault LVG *Q*-consumption is strongly dominated by the behaviour of SPIMs: they constitute more than 91% of it. *Q*-losses increase during and after the fault, and *Q*-production of SMPS-loads increases during the fault. The use of PV-systems increases the *Q*-consumption of SPIMs, and decreases the *Q*-production of SMPS-loads and *Q*-losses almost over the complete time horizon, Figure 7b).

DVS upgraded PV-systems inject reactive power into the grid during the fault, Figure 7c). The corresponding post-fault stabilization process is characterised by a distinct oscillation of the SPIMs' and PV-systems' *Q*-contribution: the maximum values of 188kvar inductive and 100kvar capacitive are reached at t =248ms and t =240ms, respectively. Figure 8 shows the voltage profiles of both

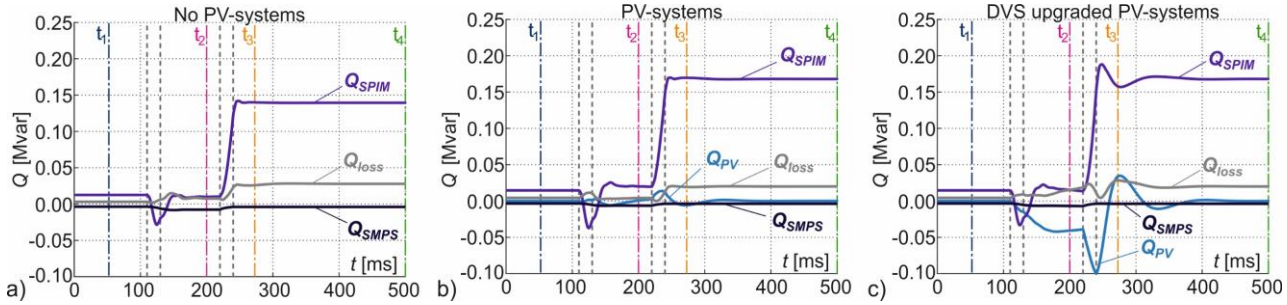

Figure 7. *Q*-consumption or -injection of different devices for different scenarios: a) no PV-systems; b) PV-systems; c) DVS upgraded PV-systems.

feeders for different time-points and scenarios. Depending on the time, voltage profiles differ from each other. Before the fault (t_1), voltage profiles of both feeders lay within the limits in all scenarios (blue coloured). During the fault (t_2), voltage profiles lay far below the lower voltage limit in all scenarios (magenta coloured). Generally, PV-systems increase the voltage in this time period, Figure 8b) and 8c). In the DVS upgraded case, this increase is smaller, Figure 8c). Voltage profiles for the time-points t_3 and t_4 are yellow and green coloured, respectively. Without PV-systems, the LVG behaviour quickly stabilizes after the fault, thus the corresponding voltage profiles overlay each other, Figure 8a). The lower voltage limit is violated by both feeders,

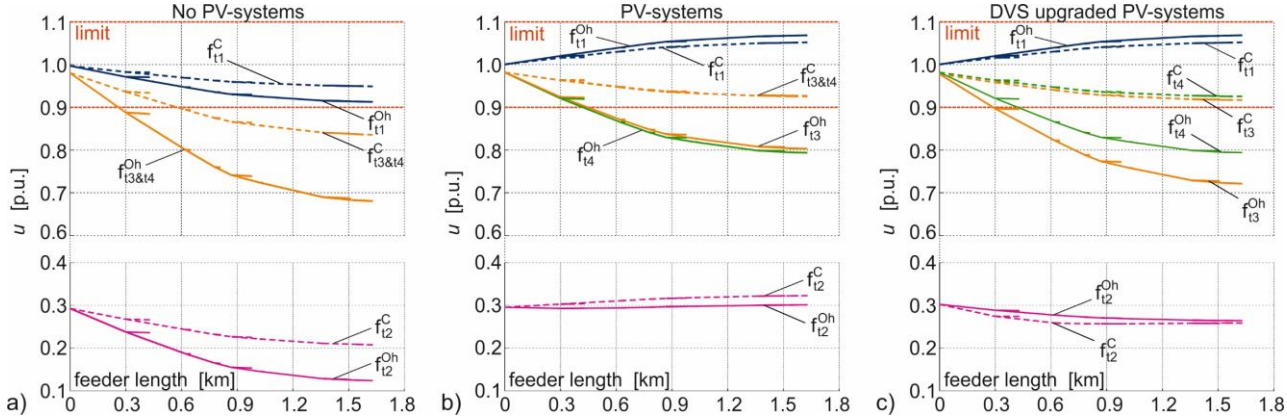

Figure 8. Voltage profiles of both feeders for different time-points and scenarios: a) no PV-systems; b) PV-systems; c) DVS upgraded PV-systems.

especially by the overhead line one. The active power injection of PV-systems provokes the alleviation of the voltage limit violations along the cable feeder, because of its high R/X ratio (2.57), Figure 8b) and 8c). Contrarily, at the overhead line feeder (with an R/X ratio of 0.92), the lower voltage limit is violated. In the case of DVS upgraded PV-systems, the limit violation at t_3 is larger than that at t_4, because of the oscillating reactive power flow.

CONCLUSION

During a fault in the superordinate grid, LVGs with a large number of DVS upgraded PV-systems inject reactive power into it, supporting its voltage recovery process. Paradoxically, in this case LVG voltages are lower compared to the case where PV-systems are not DVS upgraded.

During and after the voltage recovery process, LVGs with a large number of DVS upgraded PV-systems are subject to damped reactive power oscillations. Consequently, also the superordinate grid is subject to oscillations which may be dangerous in distinct conditions. Therefore, the investigation of the superordinate grid's (MVG) behaviour in presence of LVGs with a large number of DVS upgraded PV-systems is necessary to clarify the development of the reactive power oscillations.

ACKNOWLEDGMENT

This work is done as part of DeCAS-Project, which has received funding in the framework of the joint programming initiative ERA-Net Smart Grids Plus, with support from the European Union's Horizon 2020 research and innovation program.

REFERENCES

[1] EON Netz GmbH, "Grid Code: High and Extra High Voltage", Bayreuth, April 2006

[2] IEEE Std 1547–2018, "Standard for Interconnection and Interoperability of Distributed Energy Resources with Associated Electric Power Systems Interfaces", 2018

[3] A. M. Azmy and I. Erlich, "Impact of distributed generation on the stability of electrical power system," *IEEE Power Engineering Society General Meeting*, 2005, San Francisco, CA, 2005, pp. 1056-1063 Vol. 2.

[4] Carson W. Taylor, "Power System Voltage Stability", McGraw-Hill Inc., 1994 ISBN: 0-07-063184-0

[5] CIGRE Working Group C4.605, "Modelling and Aggregation of Loads in Flexible Power Networks", February 2014

[6] NERC, "A Technical Reference Paper: Fault-Induced Delayed Voltage Recovery", June 2009

[7] P. Irminger *et al.*, "Air conditioning stall phenomenon - Testing, model development, and simulation," *PES T&D 2012*, Orlando, FL, 2012

[8] Paul C. Krause et al., "Analysis of Electric Machinery and Drive Systems", Second Edition, Wiley Inter-Science, 2002

[9] M. Z. C. Wanik, A. A. Ibrahim, A. K. M. Hussin, M. R. Rusli and J. H. Tang, "Simplified dynamic model of photovoltaic generation system for grid integration studies," *2014 5th International Conference on Intelligent and Advanced Systems (ICIAS)*, Kuala Lumpur, 2014, pp. 1-6.

[10] R. Teodorescu, M. Liserre, P. Rodríguez, "Grid Converters for Photovoltaic and Wind Power Systems", 2011 John Wiley & Sons, Ltd.

APPENDIX

Table 1 shows the parameters which are used for the SPIM model; they are based on reference [7]. The winding parameters can be calculated by multiplying the normalized values from Table 1 with R_{base} and L_{base}.

Table 1: Parameters of SPIM model

Rated power	($P_{n,SPIM}$)		500 W
Rated voltage	($U_{n,SPIM}$)		230 V
Rated frequency	($f_{n,SPIM}$)		50 Hz
Turn ratio	(n)		1.18
Pole pairs	(p)		1
Inertia	(H)		0.03 s
Main winding		**Auxiliary winding**	
r_s	0.0539	r_S	0.0572
r'_r	0.0653	r'_R	0.0910
l_{ls}	0.1016	l_{lS}	0.1262
l'_{lr}	0.1016	l'_{lR}	0.1415
l_{ms}	2.7277	l_{mS}	3.7980

$$R_{base} = \frac{U^2_{n,SPIM}}{P_{n,SPIM}}; \qquad L_{base} = \frac{R_{base}}{2\pi \cdot f_{n,SPIM}} \tag{3}$$

The mechanical torque is set to a constant value of $T_m = 0.7$ Nm per SPIM. The run capacitor is set to $C_{run} = 6.1$ µF, which means the SPIMs have a rated power factor of approximately 0.9 inductive. Start-capacitor is not considered, since in this paper SPIMs are initialized with 100% of rated speed, thus the start-capacitor does not affect the simulations [7]. In Tables 2 and 3 are shown the positive sequence specific resistance $R'_{(1)}$, inductance $L'_{(1)}$ and capacitance $C'_{(1)}$, as well as the zero sequence ones, $R'_{(0)}$, $L'_{(0)}$ and $C'_{(0)}$.

Table 2: Parameters of cables

Type	$R'_{(1)}$; $R'_{(0)}$	$L'_{(1)}$; $L'_{(0)}$	$C'_{(1)}$; $C'_{(0)}$
	Ω/km	mH/km	µF/km
4x50 Al	0.641;1.590	0.271;3.244	0.720;0.432
4x150 Al	0.206;0.672	0.255;1.238	1.040;0.624

Table 3: Parameters of overhead lines

Type	$R'_{(1)}$; $R'_{(0)}$	$L'_{(1)}$; $L'_{(0)}$	$C'_{(1)}$; $C'_{(0)}$
	Ω/km	mH/km	µF/km
4x50 Al	0.615;1.846	1.198;4.193	0.015;0.008
4x95 Al	0.326;0.979	1.132;3.963	0.015;0.008